Arch. Metall. Mater. **68** (2023), 2, 591-598

DOI: https://doi.org/10.24425/amm.2023.142439

K.K. FENG[1], Y.L. YI[1*], Y. QIN[1], H.R. JIN[2,3*]

PREPARATION PROCESS OF COATING INTERLAYER AND THE PERFORMANCE OF EH40/2205-CLAD PLATE WITH INTERLAYER

This study aimed to investigate the effect of different coating processes on interlayer coating using ProCAST software and identify the preferred coating process so as to prepare an EH40/2205 composite plate with a coating interlayer of Ni-5 Fe-15 Co (wt.%) displaying good performance. The preparation and characterization tests were conducted to analyze the interlayer coating, the diffusion of elements at the bonding interface and the mechanical properties of the hot-rolled composite plate. The results showed that the coating rate increased linearly with an increase in the initial coating temperature, pressure difference and the width ratio of the suction layer. The interlayer coating was complete under the guidance of optimized process parameters, and the test results and simulations confirmed each other. The coated interlayer successfully blocked the diffusion of elements between the bonding surfaces. The tensile strength of the rolled composite plate was 580 MPa, which met the needs of the project. The tensile shear fracture occurred at EH40, which proved that the plate was well bonded.

Keywords: Element diffusion; interlayer coating; mechanical properties; numerical simulation; stainless steel-clad plate

1. Introduction

The 2205/EH40 composite plates are widely used in petroleum, transportation and other industries because of the corrosion and wear resistance of duplex stainless steel, and the high strength and processability of low-carbon steel [1-3]. Adding an appropriate interlayer in the composite plate can restrict the diffusion of interface elements [4]. However, the introduction of an interlayer has a great impact on the bonding performance of the composite plate.

Nowadays, an interlayer metal in plate, sheet, foil, film and other states is added to a composite plate by embedding, spraying, electroplating, chemical plating, vapor deposition, and other methods [5-7]. Balasubramanian [8] added a silver interlayer to titanium and 304 stainless steel through solid embedding. Zu et al. [9] used a thermal spraying method to introduce an Ag-based composite material into the sandwich to prepare a stainless steel composite plate. Although interlayers are added to block element diffusion using these methods, the interlayer vacuum is still difficult to control after welding encapsulation and long-term vacuum treatment [10]. The interlayer vacuum coating technology involves heating the interlayer material to a molten state in a vacuum environment, filling the alloy solution into the composite plate by vacuum differential pressure, and finally forming an interlayer by cooling and curing. This method can extrude the remaining gas and effectively improve the interlayer vacuum [11,12]. However, owing to the interlayer thickness, an unreasonable coating process leads to insufficient pouring and incomplete coating of the interlayer. In the field of metallurgical formation, some scholars have studied the quality of thin-sheet formation. Yang et al. [13] successfully prepared an Ni_3Al-based IC10 superalloy thin plate by directional solidification technology. Li et al. [14] examined the influence of drawing speed on the formation of a liquid steel sheet. In conclusion, the metal fluidity is the premise to guarantee the coating quality of the interlayer in the process of coating. The interlayer metal fluidity can be improved by adjusting the interlayer alloy ratio. Meanwhile, due to the change in the interlayer alloy ratio, the corresponding optimal coating process parameters should be selected.

This study, involved the use of coating interlayer composite plates as the research object. We used the numerical simulation

[1] YANSHAN UNIVERSITY, SCHOOL OF MECHANICAL ENGINEERING, QINHUANGDAO, CHINA
[2] YANSHAN UNIVERSITY, KEY LABORATORY OF ADVANCED FORGING & STAMPING TECHNOLOGY AND SCIENCE OF MINISTRY OF NATIONAL EDUCATION, QINHUANGDAO, CHINA
[3] YANSHAN UNIVERSITY, PARALLEL ROBOT AND MECHATRONIC SYSTEM LABORATORY OF HEBEI PROVINCE, QINHUANGDAO, CHINA
* Corresponding authors: yiyali@ysu.edu.cn, ysujhr@ysu.edu.cn

method combined with experiments to explore the influences of the coating process parameters such as initial coating temperature, coating pressure differential, and suction layer width ratio (the ratio of the suction diameter to the interlayer width) on the interlayer of EH40/2205 stainless steel composite plates with high fluidity ratio, and to develop appropriate optimized coating procedures. The coating tests were completed according to the optimized coating procedures. The interfacial element diffusion and mechanical properties of rolled 2205/Fe-Co-Ni/EH40 stainless steel composite plates were detected and analyzed through metallographic observation, hardness measurement, scanning electron microscopy, and energy spectrum analysis.

2. Experimental and methods

2.1. Establishment of the finite element model

The numerical simulation was conducted using ProCAST. The three-dimensional model was constructed according to the interlayer vacuum coating mold and meshed. The detailed dimensions are shown in Fig. 1. The gravity acceleration was 9.8 m/s^2, the heat transfer coefficient was 4 kW/(m^2·°C), the initial mold temperature was 20°C, the cooling water temperature was 15°C, the mold outer wall cooling mode was air cooling, and the overall simulation parameter was gravity coating.

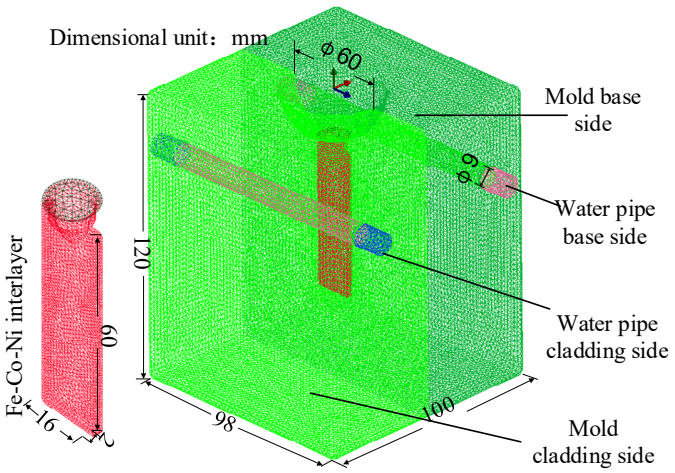

Fig. 1. Three-dimensional modeling of the mold

2.2. Influence of process parameters on interlayer formation

2.2.1. Influence of the initial coating temperature on interlayer formation

The differential pressure of the coating was 85 kPa, the width ratio of the suction layer was 0.5, and the initial coating temperature were 1550°C, 1600°C, 1650°C, and 1700°C. The interlayer forming conditions under different initial coating temperatures are shown in Figs 2 and 3. As shown in the figures, when the initial coating temperature was 1550°C, the temperature of the melt dropped sharply after contacting the wall surface, so that the melt solidified and crystallized on the wall surface soon after it entered the interlayer. When the initial coating temperature was 1600°C, the viscosity and surface tension values decreased, and the melt coating area gradually expanded. When the initial coating temperature reached 1650°C, the melt rose from both sides along the wall after touching the bottom surface because the front end of the melt had a high speed and the inertia was greater than the propulsion resistance, and finally the melt was completely coated. When the initial coating temperature reached 1700°C, the nonuniform temperature distribution was observed between layers. Also, the flow state was turbulent, which was not conducive to the timely feeding of the subsequent melt.

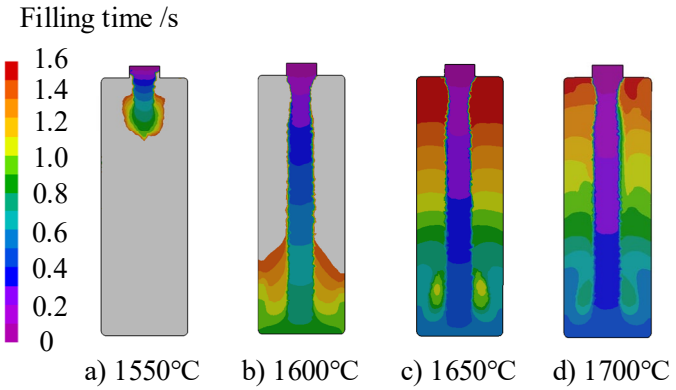

Fig. 2. Coating process at different initial coating temperatures

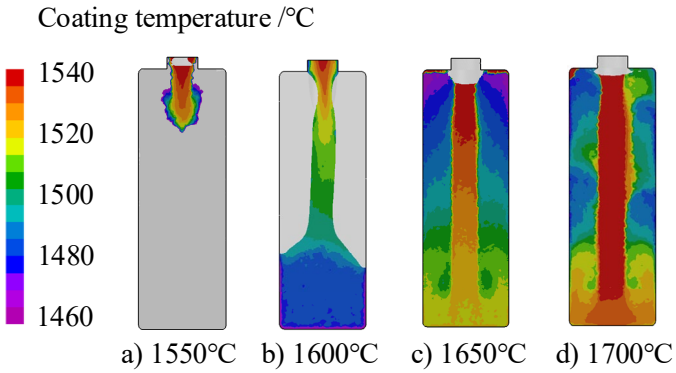

Fig. 3. Temperature field at different initial coating temperatures

The forming quality of the fully coated interlayer at 1650°C and 1700°C was further analyzed from the perspective of interlayer shrinkage (Fig. 4). Most of the shrinkage cavities were concentrated near the bottom of the interlayer, and the shrinkage cavity ratio owing to the coating interlayer being greater than 1650°C at 1700°C, which proved that the coating interlayer by the melt in turbulent flow led to more shrinkage cavities in the interlayer. In conclusion, an increase in the initial coating temperature effectively improved the coating rate of the interlayer; however, a very high temperature increased the shrinkage cavity rate of the interlayer, thus affecting its forming quality.

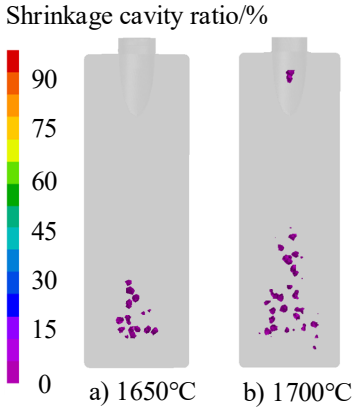

Fig. 4. The shrinkage cavity ratio of interlayer at 1650 and 1700°C

2.2.2. Influence of the difference in the coating pressure on interlayer formation

The initial coating temperature was 1600°C, the width ratio of suction layer was 0.375, and the coating pressure differences were 70 kPa, 75 kPa, 80 kPa, and 85 kPa. Interlayer forming under different coating pressures is shown in Figs 5 and 6.

Figs 5 and 6 show that when the coating pressure difference was 70 kPa, the melt driving force was insufficient, which solidified the melt, crystallized on the wall surface, and blocked the inner melt coating, resulting in breakpoints in the coating process. The coating rate of the interlayer increased gradually increase in the coating pressure difference.

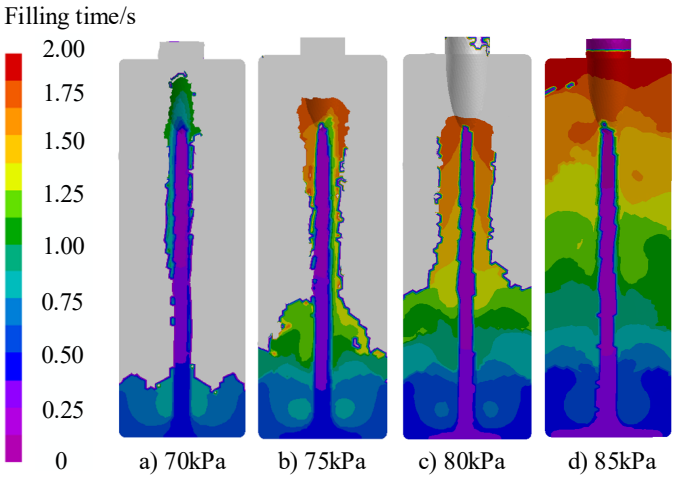

Fig. 5. Coating process at different coating pressures

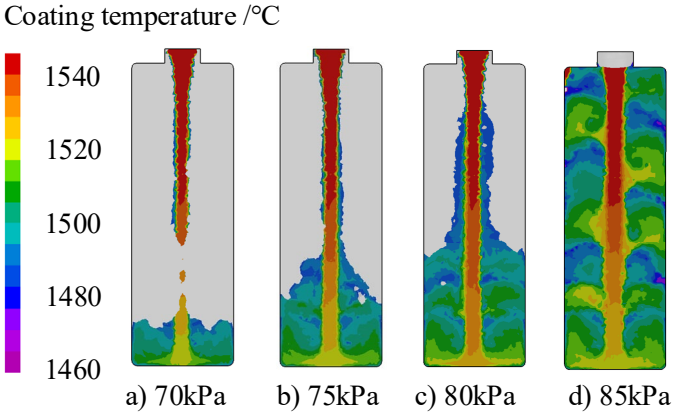

Fig. 6. Temperature field at different coating pressures

2.2.3. Influence of the suction layer width ratio on interlayer formation

The initial coating temperature was 1650°C, the coating pressure difference was 85 kPa, and the width ratio of the suction layers were 0.250, 0.375, 0.500, and 0.625. The forming condition of the interlayer under different suction layer width ratios is shown in Figs 7 and 8.

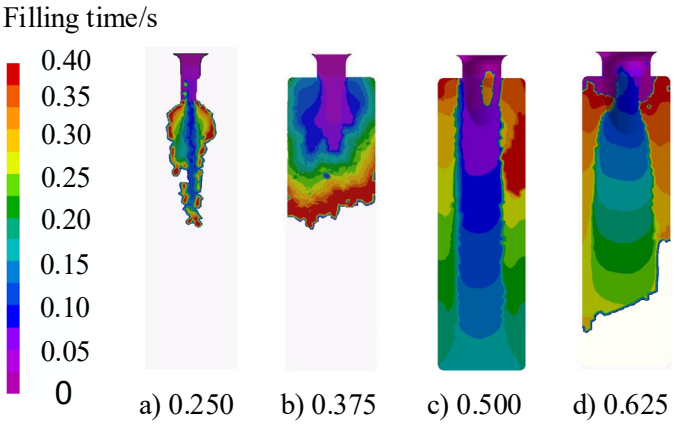

Fig. 7. Coating process at different suction layer width ratios

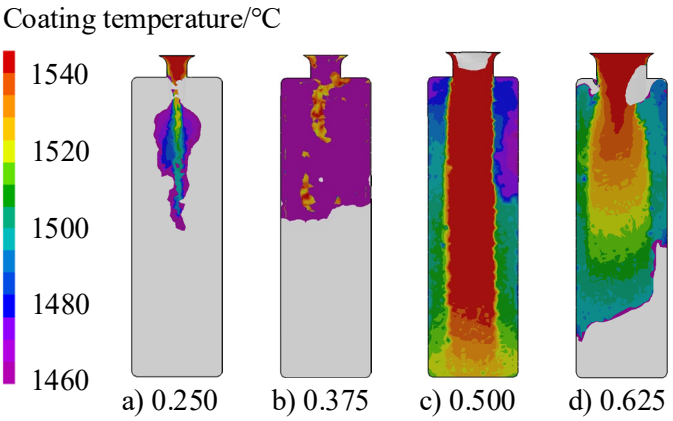

Fig. 8. Temperature field at different suction layer width ratios

Figs 7 and 8 show that when the width ratios of the suction layers were 0.250 and 0.375, solidification and crystallization occurred at the front end of the melt and could not be coated downward. Hence, it spreads towards the width and finally stopped coating. When the width ratio of the suction layer increased to 0.500, the interlayer was completely coated, and when it continued to increase to 0.625, the coating rate of the interlayer decreased. This was due to the increase in the width ratio of the suction layer, which reduced the propulsion force at the front end of the melt. Overall, when the width ratio of

the suction layer was less than 0.500, the increase in the width ratio of the suction layer helped in increasing the coating rate of the interlayer. However, the coating rate began to decline after the suction layer width ratio increased again.

2.2.4. Establish ment of the technological parameters of the interlayer coating

The coating rate was taken as the prerequisite element in the molding index to obtain high-quality interlayer coating, and the orthogonal test was designed. According to the results of 100% coating rate obtained by preliminary simulation, the level factors of initial coating temperature, coating pressure difference and suction layer width ratio were selected. Three horizontal factors were selected for each factor (TABLE 1).

TABLE 1

Orthogonal test table of three factors and three levels

Factor	Level 1	Level 2	Level 3
Initial coating temperature (°C)	1600	1650	1700
Differential pressure of coating (kPa)	80	83	85
Width ratio of suction layer	0.4	0.5	0.6

The coating simulation under different coating process parameters was carried out according to TABLE 1. The interlayer coating quality was evaluated using the interlayer shrinkage rate. The simulation results and analysis are shown in TABLES 2 and 3. An analysis of the range R in the table showed that the factors affecting the shrinkage rate of the interlayer were coating pressure difference, initial coating temperature and suction layer width ratio in primary and secondary orders. The lower the index value of the coating rate, the better the coating quality of the interlayer. Therefore, the horizontal factor corresponding to the lower value of k should be selected. The optimal coating scheme could be obtained using this method: the initial coating temperature was 1650°C, the coating pressure difference was 85 kPa, and the width ratio of the suction layer was 0.5.

TABLE 2

Orthogonal test results of the coating rate

Project	Initial coating temperature (°C)	Coated with differential pressure (kPa)	Width ratio of suction layer	Shrinkage rate (%)
Test 1	1600	80	0.4	23.14
Test 2	1600	83	0.5	9.63
Test 3	1600	85	0.6	9.89
Test 4	1650	80	0.5	5.99
Test 5	1650	83	0.6	5.34
Test 6	1650	85	0.4	5.82
Test 7	1700	80	0.6	8.91
Test 8	1700	83	0.4	10.78
Test 9	1700	85	0.5	6.84

TABLE 3

Analysis of test results

Indicators	Initial coating temperature index	Coating pressure difference index	Suction layer width ratio index
K_1	42.66	38.04	39.74
K_2	17.15	25.75	22.46
K_3	26.53	22.55	24.14
k_1	14.22	12.68	13.25
k_2	5.72	8.58	7.49
k_3	8.84	7.52	8.05
R	8.50	5.16	5.76

Note: K_i is the sum of test index values corresponding to each factor at level i. k_i is the average melt flow coefficient of each factor at level i, which was used to infer the optimal level of each factor. R is the range of shrinkage cavity ratio at different levels. The greater the range R, the more significant the influence is on the shrinkage cavity ratio of the interlayer.

2.3. Test materials and methods

2.3.1. Melting and coating test

The material particles of Ni-5 Fe-15 Co(wt.%) (the purity of the particles used was 99.95%) were weighed. The total mass of the material was 45 g. The weighing error of each metal particle was ±0.002 g. The vacuum melting and coating tests were conducted using the NMS-DRXXII ingot mold rotating vacuum arc melting/casting system according to the optimized process parameters. The fully coated filling interlayer was obtained (Fig. 9).

Fig. 9. Coating interlayer under a preferred process

2.3.2. Test of rolling

During the rolling process of the clad plate, the traditional rolling method was prone to deformation instability owing to the large difference in the deformation resistance of the materials of each layer. Therefore, the symmetrical rolling composite method (base layer-intermediate interlayer-cladding-isolating agent-cladding-intermediate interlayer-base layer) was developed. At the same time, a high-temperature isolating agent (distilled water, anhydrous ethanol, and silicon dioxide in the ratio of 5:3:2) in two symmetrical planes (2205 stainless steel surface) was sprayed for

TABLE 4

Chemical compositions of component materials (mass fraction, %)

Material	C	Si	Mn	P	S	Ni	Cr	Mo	Al	Cu	Fe
EH40	0.158	0.33	1.01	0.015	0.002	0.01	0.01	0.005	0.045	0.04	Bal.
2205	0.02	0.61	1.10	0	0	5.12	23.04	3.12	—	—	Bal.

the separation of the symmetrical arrangement of the composite plate after rolling. The assembly method is shown in Fig. 10. Using two high-speed mills, five-pass vacuum hot rolling tests were conducted on the coated formed slabs. The rolling reduction rates were 20%-10%-10%-10%-10%. The rolling speed was 40 mm/s, and the initial rolling temperature was 1200°C. The material component parameters are shown in TABLE 4.

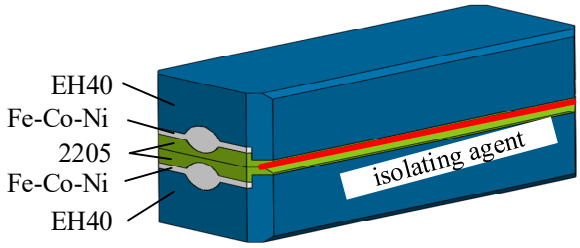

Fig. 10. Group billet

After rolling, the composite plate samples were separated. The tensile specimen, tensile shear specimen and metallographic specimen were prepared. The hardness test, optical microscope (OM), scanning electron microscope (SEM), and energy dispersive spectrometer (EDS) were used to observe the interface microstructure and analyze the diffusion of interface elements. The overall mechanical properties of the sheet were tested using tensile test, tensile shear test, and fracture analysis.

3. Results and Discussion

3.1. Characterization of composite plate prepared by hot rolling

The interface morphology of a composite plate after hot rolling was obtained using a metallographic microscope (Fig. 11). Fig. 11(a) shows that the composite interface after rolling was flat and straight, and no defects, such as pores and casting holes, were observed in the interlayer. Fig. 11(b) shows that EH40 was well bonded to the interlayer with a clear interface and no obvious decarburization occurred. Ferrite and pearlite were distributed randomly on the side of EH40 low-carbon steel. Equiaxed ferrite was distributed on the side close to the boundary. The grain refinement on the EH40 side increased along the thickness direction toward the bonding interface owing to the difference in the degree of deformation. Fig. 11(c) shows that the γ phase austenite was distributed on the α-phase ferrite matrix in 2205 stainless steel. The interface was well bonded at the junction with the interlayer. In summary, the Fe-Cobalt-Nickel interlayer effectively blocked the diffusion of carbon elements from the EH40 side to the 2205 dual-phase stainless steel side.

The ferritic region on the carbon steel side was the weakest position near the composite interface. Carbon chromium compounds were easily formed in this region and could easily become the crack source of shear fracture and reduce the strength of the composite plate [15]. The hardness of the bonding interface was measured, and the results are shown in Fig. 12. The average hardness of 2205 duplex stainless steel was nearly 352 HV, that of Fe-Cobalt-Nickel interlayer was nearly 200 HV, and that of EH40 low-carbon steel was nearly 180 HV. The hardness of the EH40 low carbon steel side of interface 2 decreased, and the hardness of the interlayer side of interface 2 increased. At a distance from interface 2, the hardness of the interlayer side gradually decreased and stabilized to the average hardness. This was due to the element diffusion of carbon at the interface, which led to the decarburization of EH40. The hardness value decreased, while the hardness on the interlayer side increased. According to the hardness distribution, the diffusion distance of the carbon element was lesser than the interlayer thickness, and it did not combine with chromium in 2205 duplex stainless steel to form a carbochrome compound.

The composition and distribution of the interface elements obtained using line scanning are shown in Fig. 13. All elements

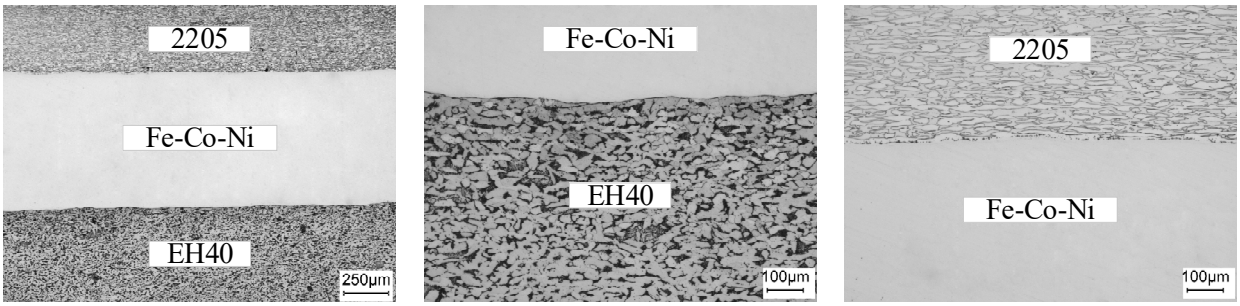

(a) Interlayer (b) Base/interlayer (c) Clad/interlayer

Fig. 11. Combination with interfacial microstructure

in the line scan result were continuous, which proved that the plates were well combined. According to the analysis of 2205 duplex stainless steel and the Fe-Co-Ni interlayer, a transition layer of chromium content was present. The length of the transition layer was nearly 15.6 μm, indicating that chromium diffusion occurred. However, the diffusion distance was lesser than the interlayer thickness. Therefore, introducing the interlayer could effectively block the diffusion of chromium.

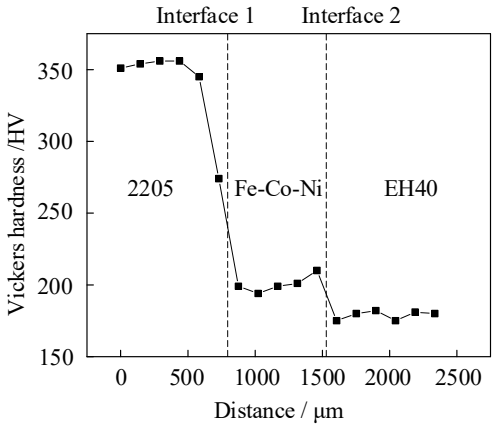

Fig. 12. Interfacial hardness distribution

The bonding interface was framed in the SEM image for surface scanning to further confirm the diffusion degree of the chromium element (Fig. 14). The analysis of the chromium distribution in Fig. 14(e) shows that the coating interlayer blocked the diffusion of chromium to EH40 low-carbon steel. Additionally, the surface scanning results, revealed no distribution of oxygen elements at the bonding interface, which proved that the high purity of the bonding interface obtained using the interlayer vacuum coating method.

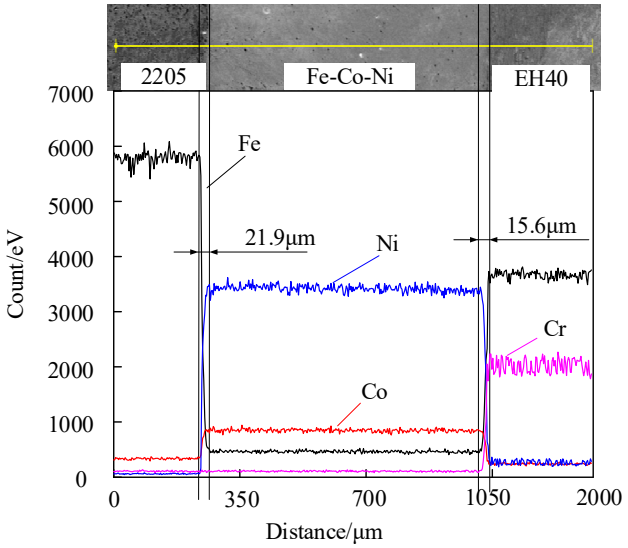

Fig. 13. Composition and distribution of interface elements

3.2. Mechanical properties of the composite plate prepared by hot rolling

The tensile stress-strain curve (Fig. 15) was drawn based on the tensile test results. The curve showed that the tensile strength of the rolled sheet was 580 MPa. The sample broke when the engineering strain was nearly 23.7%. According to GB/T 712-2011 "Ship and ocean engineering structural steel," the mechanical properties of the rolled composite plate were higher than the corresponding standard of EH40 low-carbon steel.

Similarly, the stress-strain curve was calculated and drawn based on the tensile and shear test data (Fig. 16). The curve had an obvious mutation point at the rupture, and the ultimate shear strength reached 403 MPa.

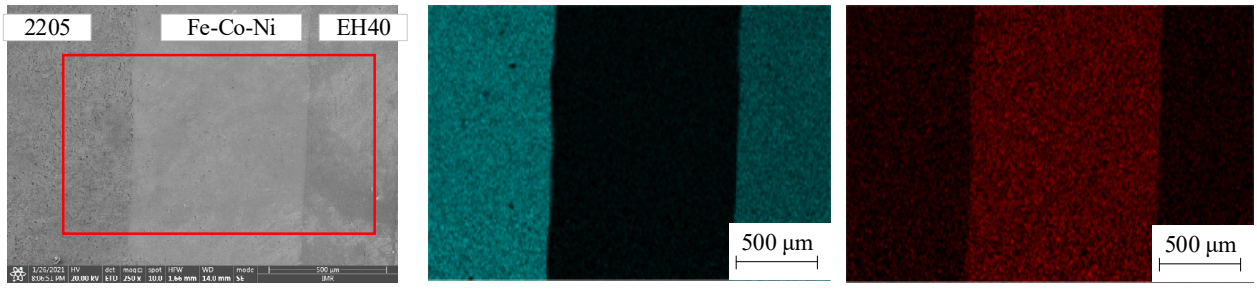

a) Combined with SEM image of interface
b) Fe element distribution
c) Co element distribution

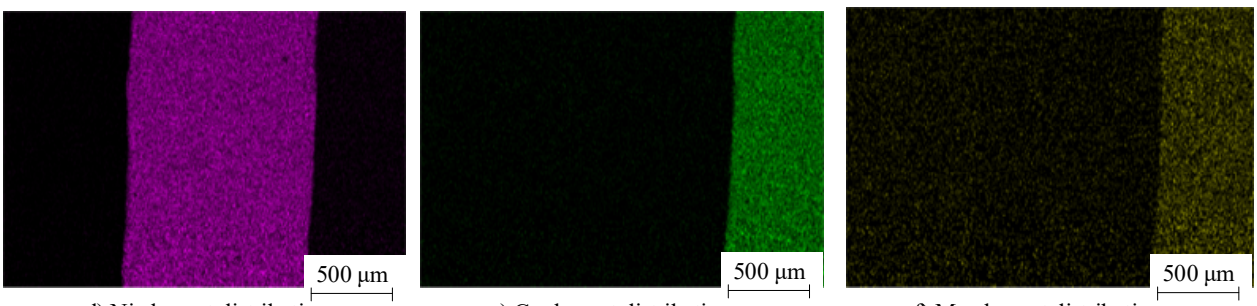

d) Ni element distribution
e) Cr element distribution
f) Mn element distribution

Fig. 14. Distribution of interface elements

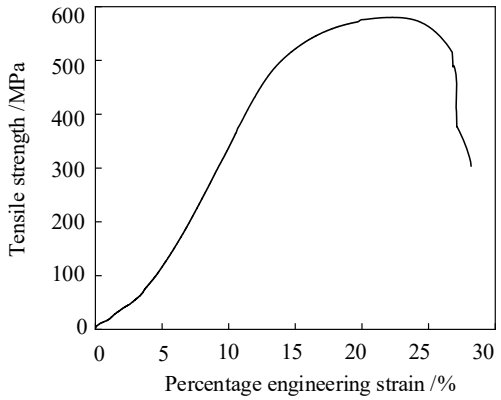

Fig. 15. Tensile stress-strain curve

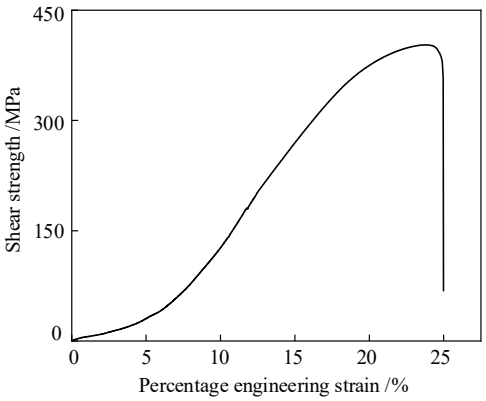

Fig. 16. Tensile shear stress-strain curve

SEM analysis of the tensile shear fracture is shown in Fig. 17. Numerous dimples were distributed on the surface of the fracture, indicating that the plate had a ductile fracture. The material at the fracture was EH40 as the matrix, and certain carbon and nickel element compounds were found at the fracture position, which proved that the composite plate bonded under this rolling process with high bonding strength.

The metallographic analysis of the fracture is shown in Fig. 18, which indicated that the EH40 structure at the fracture of the pull-shear sample was elongated. It showed that the fracture occured in EH40 low-carbon steel.

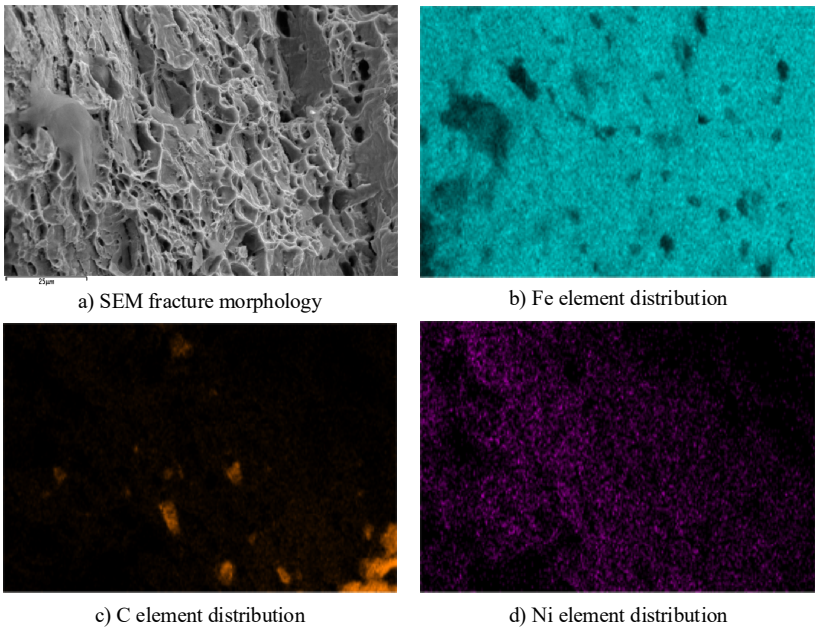

Fig. 17. Fracture morphology

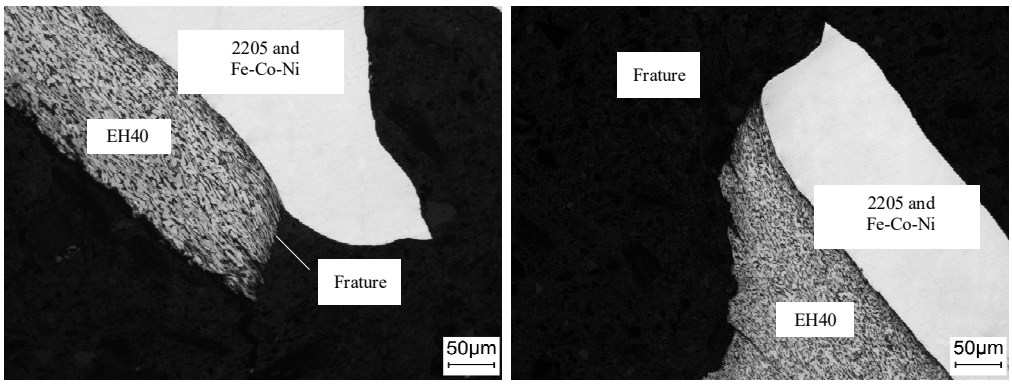

Fig. 18. Fracture microstructure

4. Conclusions

In this study, the vacuum coating process parameters were optimized using numerical simulation. The accuracy of simulation results was verified through experiments. The mechanical properties of composite plates prepared using the interlayer vacuum coating technology were tested using the rolling test and post-rolling characterization test. The conclusions were as follows:

(1) During the coating process, the coating rate increased first and then decreased with an increase in the width ratio of the suction layer. The coating rate increased with an increase in the difference between the initial coating temperature and coating pressure. However, high temperature and coating pressure differences increased the shrinkage cavity ratio and stress value of the interlayer.

(2) The orthogonal test method was used to optimize the simulation results of the coating. In the optimal coating process at the initial coating temperature of 1650°C, the coating pressure difference of 85 kPa, and the suction layer width ratio of 0.5, the filling pattern of the interlayer was complete. The coating results were verified by the experimental results. The deviation rate between the experimental and simulation values was less than 10%.

(3) The EH40/Fe-Co-Ni/2205 composite plate was prepared using the rolling test. The metallographic observation, hardness measurement, scanning electron microscopy and energy spectrum analysis showed that the thin interlayer successfully blocked the diffusion of chromium into EH40 low carbon steel at a pure interface. The tensile and tensile shear tests showed that the tensile strength of the rolled composite plate was 580 MPa, which was much higher than the national standard of 220 MPa. The shear strength was 403 MPa. The fracture position appeared at the base, and the plates were well bonded.

Acknowledgments

This study was funded by the Central Government Guide Local Scientific and Technological Development Fund Project (216Z1003G), and the Joint Fund High-end Iron and Steel Metallurgy for Natural Research Foundation Project of Hebei Province (E2020203033).

REFERENCES

[1] Rao. Sarma. Nagarjuna, et al., Influence of hot rolling and heat treatment on structure and properties of HSLA steel explosively clad with austenitic stainless steel [J], Materials Science and Technology **25** (11), 1387 (2009).

[2] K.B. Nie, Z.H. Zhu, Paul Munroe, et al., Microstructure, Tensile Properties and Work Hardening Behavior of an Extruded Mg-Zn-Ca-Mn Magnesium Alloy [J], Acta Metallurgica Sinica (English Letters) **33** (07), 922-936 (2020).

[3] O. Bouaziz, J.P. Masse, G. Petitgand, et al., A Novel Strong and Ductile TWIP/Martensite Steel Composite [J], Advanced Engineering Materials **18** (1), 56 (2016).

[4] G.Y. Zu, J.M. Yu, J.L. Wen., Effect of interlayer on interfacial bonding properties of stainless clad sheets [J], Journal of Northeastern University **24** (11), 1053-1056 (2003).

[5] X. J. Zhang, L. Li, et al., Application of insert layer in manufacturing clad metal plates [J], Steel Rolling **30** (06), 45-49 (2013).

[6] S. Kundu, S. Chatterjee., Interface microstructure and strength properties of diffusion bonded joints of titanium–Al interlayer–18Cr–8Ni stainless steel [J], Materials Science & Engineering A **527** (10), 2714-2719 (2009).

[7] Z.A. Luo, G.L. Wang, G.M. Xie, et al., Effect of Nb interlayer on microstructure and property of titanium-stainless steel clad plate bonded by vacuum hot-rolling [J], The Chinese Journal of Nonferrous Metals **23** (12), 3335-3340 (2013).

[8] M. Balasubramanian., Characterization of diffusion-bonded titanium alloy and 304 stainless steel with Ag as an interlayer [J], The International Journal of Advanced Manufacturing Technology **82** (1-4), 153-162 (2016).

[9] G.Y. Zu, J.M. Yu, J.L. Wen., Effect of Intermediate Sandwich Material and Shielding Atmosphere on Stainless Steel-Carbon Steel Bonding [J], Journal of Iron and Steel Research (01), 55-58-71 (2005).

[10] Y.L. Yi, Y.J. Kong, Y.H. Wang, et al., Effect of coating slab preparation on stainless steel/low alloy steel composite interface [J], Iron and Steel **56** (05), 105-112 (2021).

[11] H.R. Jin, Y.J. Kong, Y. Zhang, et al., Interfacial structure of 316L/EH40 clad plate with iorn-cobalt-nickel alloy as interlayer [J], Iron and Steel **55** (10), 63-68 (2020).

[12] H.R. Jin, Y. Zhang, Y J. Kong, et al., A vacuum nickel coating device and vacuum nickel coating method between vertical composite billet layers [P], Hebei Province: CN109930152B, 2020-04-28.

[13] Z.N. Yang, Z. Zhang, C.W. Guo, et al., Competitive Growth of Dendrite Arrays in the Directional Solidification of a Thin Sheet Sample [J], Rare Metal Materials and Engineering **50** (04), 1247-1253 (2021).

[14] K.K. Li, C.J. Zhang, P.C. Xiao, et al., Analysis on interface fluctuation of steel slag in mold of high casting speed thin slab continuous casting [J], Continuous Casting (01), 9-14+25 (2021).

[15] H.B. Xie, D.W. Wang, C. Yu, et al., Stainless steel/carbon steel composite plate prepared by hot-roll bonding with pure iron as intermediate material [J], Iron and Steel **52** (12), 48-53 (2017).